TWELFTH EUROPEAN ROTORCRAFT FORUM

Paper No. 42

STUDY OF THE DYNAMIC RESPONSE OF HELICOPTERS TO A LARGE AIRPLANE WAKE

Shigeru SAITO

National Aerospace Laboratory
Tokyo, Japan

Akira AZUMA, Keiji KAWACHI and Yoshinori OKUNO

Institute of Interdisciplinary Research
Faculty of Engineering, The University of Tokyo
Tokyo, Japan

September 22-25, 1986

Garmisch-Partenkirchen
Federal Repablic of Germany

Deutsche Gesellschaft für Luft- und Raumfahrt e.V. (DGLR)
Godesberger Allee 70, D-5300 Bonn 2, F.R.G.

STUDY OF THE DYNAMIC RESPONSE OF HELICOPTERS TO A LARGE AIRPLANE WAKE

Shigeru SAITO

National Aerospace Laboratory
Tokyo, Japan

Akira AZUMA, Keiji KAWACHI
and
Yoshinori OKUNO

The University of Tokyo
Tokyo, Japan

ABSTRACT

A numerical simulation of helicopter flight dynamics is performed in order to get the dynamic characteristics of helicopters which encounter a pair of trailing vortices of a preceeding large airplane, such as a jambo jet airplane. Two types of helicopter rotor, that is, articulated and hingeless types, are analyzed to make clear the effects of geometrical configuration of helicopter, rotor blade stiffness, and flight condition on the helicopter dynamic responses. The rotor aerodynamic forces which are fully coupled with the body motion with six-degrees of freedom are calculated by using the Local Momentum Theory (LMT) [1].

The time histories of the dynamic behavior of the helicopter as well as the blade motion are presented for various parameters such as the distance between helicopter and large airplane, the type of helicopter rotor, and the flight path angle with respect to the tip vortices of the large airplane.

The dynamic response of helicopter are generally moderate in comparison with those of airplane. The most severe response is given in vertical direction with almost 2g load level, and the flight path follows the shape of the vertical gust. The change of the attitudes of the helicopter depend on the flight conditions when the helicopter just hits the vortex core.

1. INTRODUCTION

When an aircraft penetrates a pair of rolled-up vortices generated by a large airplane, the aircraft is severely disturbed by the strong induced velocity surrounding and inside the vortex core in a fashion similar to that of a gust encounter [2].

Considerable analytic and experimental works have been done to predict the velocity field to the wake vortices and the dynamic behavior of a fixed wing aircraft interacting with the wake vortices [3]-[6]. However, a very few works have been devoted to the possible problem of predicting the response of a rotary wing aircraft to the vortex encounter [7]-[10]. There works mostly related to the response of helicopter penetrating the vortex with the parallel flight along the vortex core. Then it is known that the response of rolling and yawing motion of helicopter specifically having a see-saw rotor is very mild when compared to a typical response of airplane to the vortex core [11].

There are many parameters which may give some influences on the dynamic behavior of the helicopter encountering the wake vortices of large airplane. They are mass ratio, m_H/m_A, span ratio $2R/b_A$, speed ratio U_H/U_A, nondimensional separation distances X_H/b_A, y_H/b_A and z_H/b_A, flight pass angle Ψ_W and γ, hub or blade stiffness ω/Ω_H and other dynamic characteristics of the helicopter.

The sensitivity of the response to the different parameters and the effect of the simplified feedback system to alleviate the deviation from the trimmed flight on the time response of the disturbed helicopter have been partly investigated by the present authors [12],[13]. The purpose of this paper is to extend the analysis to further wide range of parameters such as an articulated rotor helicopter and a hingeless rotor helicopter flying in different flight path angles with respect to the vortex core.

2. GEOMETRY OF THE TRAILING VORTEX

The trailing vortex wake system generated by a conventional lifting wing of moderate sweep and aspect ratio is unstable and tends to roll-up to a pair of oppositely rotating trailing vortices, as shown an Figure 1. In this section, the model of a pair of trailing vortices generated by a large aircraft is described. Under the assumption that the flow is steady, axisymmetric, laminar and incompressible, and the Reynolds number of the main flow, Ux/ν where x is the axial distance, is large, the axial velocity q_x, radial velocity q_r, rotational velocity q_θ can be given by solving the Navier-Stokes' equation as follows [13],[14]:

$$\Gamma = \Gamma_0\sqrt{1 - (2y/b_A)^2} \qquad (1)$$

$$\left.\begin{aligned} q_x &= (D_0/4\pi\rho\nu_e x)\exp\{-(U_A r^2/4\nu_e x)\} = -q_x^*\exp\{-r/r^*\}^2 \\ q_r &= -(rD_0/8\pi\rho\nu_e x^2)\exp\{-(U_A r^2/4\nu_e x)\} = -q_r^*\exp\{-r/r^*\}^2 \\ q_\theta &= (\Gamma_0/2\pi r)\exp\{1-\exp\{(U_A r^2/4\nu_e x)\}\} = q_\theta^*(r^*/r)\{\exp\{-r/r^*\}^2\} \end{aligned}\right\} \qquad (2)$$

where

$$
\left.
\begin{aligned}
&\Gamma_0 = \Gamma(y=0) = (4/\pi\,\rho U_A)(L/b_A) \\
&q_x^{*} = D_0/4\pi\,\rho\,\nu_e x \\
&q_r^{*} = (rD_0/2\pi\,\rho U_A x)/r^{*2} \\
&q^{*}_{\theta} = (\Gamma_0/4\pi x)\sqrt{U_A x/\nu_e} = (\Gamma_0/4\pi)\sqrt{U_A/\nu_e}/\sqrt{x} \\
&r^{*} = 2x/\sqrt{U_A x/\nu_e} = (2/\sqrt{U_A x/\nu_e})\sqrt{x} \\
&D_0 = 2\pi\int_0^{\infty}\rho(U_A-u)urdr \cong 2\pi\int_0^{\infty}\rho U_A urdr
\end{aligned}
\right\}
\quad (3)
$$

and where D_0 and ν_e are the profile drag and the "effective eddy viscosity" rather than the kinematic viscosity respectively. The value of ν_e is given by

$$\nu_e = \nu + a\Gamma_0 \quad (4)$$

where "a" is an empirical constant, whose precise value is very difficult to define but is in the range 10^{-3} to 10^{-4} such as a = 0.0002-0.002. In this analysis, the trailing vortices are assumed to be frozen and disturbed by the blade motion.

3. MODEL ROTOR AND FLIGHT CONDITIONS

Two types of helicopter rotor are used in this paper, which are articulated and hingless rotors. The dimensions of these two rotors are shown in Table 1. As the vortex generating aircraft, Boeing 747 jambo jet airplane is used and its dimensions are shown in Table 2. Any helicopter is assumed to penetrate one of a pair of traling vortex such as the rotor hub hits the center of the vortex core with angle Ψ_W after started from an initial position (x_0,y_0,z_0) behind the airplane in the (x,y,z) coordinate as shown in Figure 1. Since both the airplane and the helicopter are moving forward with their own velocities, U_A and U_H respectively, the distance of the disturbed helicopter behind the airplane is more than xo when the rotor hub hits the center of the vortex core. The velocity components along a horizontal line passing through the core centers at the distance x = 10,000 and 2,000 m are shown in Figures 2 (a), (b) respectively by using the above mentioned trailing vortex model.

The spatial CG position of the disturbed helicopter with

$$\begin{Bmatrix} X_{CG} \\ Y_{CG} \\ Z_{CG} \end{Bmatrix} = \begin{Bmatrix} X_{CG,0} \\ Y_{CG,0} \\ X_{CG,0} \end{Bmatrix} + \begin{Bmatrix} U_A t \\ 0.0 \\ 0.0 \end{Bmatrix} + \int_0^t T_1 \cdot T_2 \begin{Bmatrix} U_{H,XB} \\ U_{H,YB} \\ U_{H,ZB} \end{Bmatrix} dt \qquad (5)$$

where T_1, T_2 are transformation matrices from the body coordinate (X_B, Y_B, Z_B) of the helicopter to the initial body coordinate $(X_{B,0}, Y_{B,0}, Z_{B,0})$, which is the body coordinate at time t = 0 and from the initial body coordinate to the airplane coordinate respectively, shown in Appendix A. The relative position of the rotor hub with respect to the vortex core coordinate (x,y,z), the origin of which is fixed to the respective wing tip, is givein by

$$\begin{Bmatrix} x_h \\ y_h \\ X_h \end{Bmatrix} = \begin{Bmatrix} x_{CG} \\ y_{CG} \\ z_{CG} \end{Bmatrix} + T_2 \cdot T_1 \begin{Bmatrix} l_R \\ 0.0 \\ h_R \end{Bmatrix} - \begin{Bmatrix} 0.0 \\ \pm b_A/2 \\ 0.0 \end{Bmatrix} \qquad (6)$$

where $(l_R, 0.0, h_R)^T$ is the hub position with respect to the body coordinate and $\pm$ denotes the left and right trailing vortices respectively.

Various flight conditions of the vortex genarating airplane and of the disturbed helicopter are given in Table 3.

4. EQUATIONS OF MOTION OF HELICOPTER

By referring to Figure 3, equations of motion of a helicopter with six-degrees of freedom can be given by [13].

$$\left.\begin{aligned} m_H \{du_H/dt + qw_H - rv_H\} &= F_{XB} \\ m_H \{dv_H/dt + ru_H - pw_H\} &= F_{YB} \\ m_H \{dw_H/dt + pv_H - qu_H\} &= F_{ZB} \end{aligned}\right\} \qquad (7)$$

$$\left.\begin{aligned} I_X dp/dt - J_{XZ}\{dr/dt + pq\} - \{(I_Z - I_Y)\} qr &= M_{XB} \\ I_Y dq/dt + J_{XZ}\{p^2 - r^2\} + \{(I_X - I_Z)/I_Y\} rp &= M_{YB} \\ I_Z dr/dt - J_{XZ}\{dp/dt - qr\} - \{(I_Y - I_X)\} pq &= M_{ZB} \end{aligned}\right\} \qquad (8)$$

where the mass (m_H), the moments of inertia (I_X, I_Y, I_Z) and the product of inertia (J_{XZ}) are those related to the helicopter body product of inertia (J_{XZ}) are those related to the helicopter body which does not include the main rotor. In equations (7) and (8), the helicopter is assumed to have a body of symmetric configulation. The external forces (F_{XB}, F_{YB}, F_{ZB}) and moments (M_{XB}, M_{YB}, M_{ZB}) are given from the main rotor through the hub, a tail rotor, horizontal and vertical stabilizer and a fuselage. Detailed expression of those forces and moments are given in Appendix B.

The blade motion is considered to be the flapping motion and the lead-lag motion about the respective articulated hinges. For the hingeless rotor, both the flapping and lead-lag motions about eqivalent flapping and lead-lag hinges respectively are considered in this analysis as follows:

$$I_\beta \ddot{\beta} + M_\beta \Omega^2 \beta - R^2 \int_{x_\beta}^{1} l(x - x_\beta)dx + k_\beta(\beta - \overline{\beta}_0) = 0.0 \quad (9)$$

$$I_\zeta \ddot{\zeta} + k_\zeta \Omega \dot{\zeta} + M_\zeta \Omega^2 \zeta - R^2 \int_{x_\zeta}^{1} d(x - x_\zeta)dx$$
$$+ k_\zeta(\zeta - \overline{\zeta}_0) - 2R^2 \int_{x_\zeta}^{1} (x - x_\zeta)(x - x_\beta)\Omega \beta \dot{\beta}\, dm = 0.0 \quad (10)$$

The aerodynamic forces and moments at the rotor hub are calculated by the LMT in which the spanwise and azimuthwise steps are performed by $\Delta x = r/R = 1/20$ and $\Delta\psi = 10°$ respectively. The induced velocity generated by airplane is considered to be a given gust velocity and is also disturbed by the blade motion of the helicopter [12],[13]. The blade motion and the body motion of the helicopter are calculated by the Runge-Kutta method. The timewise increment of the computation is $2\pi/360\Omega$ second.

5. SIMPLIFIED LOAD ALLEVIATION SYSTEM

When the helicopter penetrates a three-dimensional gust field, the thrust response is strongly affected by the vertical velocity [15]. To reduce the response, two simplified load alleviation systems are applied. One is the Flapping Suppression System (FSS) [16],[17] and the other is the Simplified Feedback System (SFS) such as the automatic stability equipment [18],[19].

The FSS is one of the active load alleviation system, in which the deviation of the flapping angle is fedback to the individual blade pitch in the form of

$$\theta_i = \theta_{0i} + \theta_{1Si}\sin\psi_i + \theta_{1Ci}\cos\psi_i + \Delta\theta_i \quad (11)$$

$$\Delta\theta_i = k_\beta \Delta\beta + k_{\dot\beta} \Delta\dot\beta + k_{\ddot\beta} \Delta\ddot\beta$$

(i denotes the i-th blade)

In Reference 16, the reduction rate of the thrust deviation by the vertical gust became 50 to 70 % by using an appropriate combination of feedback gains.

In the SFS, the deviations of the body motion, for example, linear acceleration, velocity, attitude deviations of the helicopter are fedback to the collective, longitudinal and lateral pitch controls. In this paper, the Attitude Hold System and the Velocity Hold System are applied to maintain the attitude and the flight velocity of the helicopter. The values fedback to the pitch angle of the blade are as follows:

collective pitch angle,

$$\Delta\theta_0 = G_{\dot{\overline{\Delta h}}} \dot{\overline{\Delta h}} + G_{\ddot{\overline{\Delta h}}} \ddot{\overline{\Delta h}}$$

longitudinal cyclic pitch angle,

$$\Delta\theta_{1S} = G_\Theta(\Theta - \Theta_0) + G_{\dot\Theta}\dot\Theta - G_{\overline{\Delta U}_X}(\overline{\Delta U}_X) - G_{\dot{\overline{\Delta U}}_X}(\dot{\overline{\Delta U}}_X)$$

lateral cyclic pitch angle,

$$\Delta\theta_{1C} = - G_\Phi(\Phi - \Phi_0) - G_{\dot\Phi}\dot\Phi - G_{\overline{\Delta U}_Y}(\overline{\Delta U}_Y) - G_{\dot{\overline{\Delta U}}_Y}(\dot{\overline{\Delta U}}_Y)$$

tail rotor collective pitch angle,

$$\Delta\theta_{0T} = - G_\Psi(\Psi - \Psi_0) - G_{\dot\Psi}\dot\Psi \qquad (12)$$

where $G_{(\ )}$ denotes the feedback gain and suffix (0) denotes the trimmed value. The velocity and acceleration are nondimensionalized by $R\Omega$ and $R\Omega^2$ respectively. Each feedback gain is determined by the stability analysis by means of the root locus method. The block diagrams for each control system are shown in Figures 4 (a), (b), (c).

6. NUMERICAL SIMULATION

In this section, the results of the dynamic response of the helicopter are presented and discussed. In the numerical simulations, the dynamic behaviors of the helicopter were firstly calculated for various combinations of the helicopter control inputs. The dynamic behavior of the trimmed flight is considered to be a good reference to the disturbed flight of the helicopter. The responses of helicopter with a see-saw rotor was precisely discussed in References [12] and [13].

6-1 Response of helicopter with articulated rotor

In this section, let us consider the dynamic responses of the helicopter with articulated rotor penetrating the vortex wake of the large airplane. The detailed dimensions and flight conditions of this helicopter are given in Table 1 and 3 respectively. Compared with the helicoper with see-saw rotor, the rotor size and the body size are fairly small.

Before performing the calculation of the disturbed flight, the calculations of the dynamic response were examined in order to find the control inputs for the trimmed flight. The vibratory characteristics are reduced in comparison with those of the helicopter with see-saw rotor given in References [12] and [13] because of four blades instead of two.

Shown in Figures 5 (a),(b) and (c) are the time responses of this helicopter flying with the climbing angle of 10° for the normal (Ψ_W=90°), the diagonal (Ψ_W=30°) and the parallel (Ψ_W=0°) penetrations respectively. The Figure 5 are not identical to those presented in reference [13]. In the present case, the helicopter is considered to fly under uncontrolled state either manually or automatically to compensate the yawing moment. Compared with the case of the see-saw rotor, the shape of the responses is appreciably different.

In the normal penetration, the thrust response of the rotor is very mild. Even though the helicopter flies with climbing angle of 10° , the helicopter seems to hit the second vortex core as shown in Figure 5 (a). This is because the helicopter excursions are very high and the attitude deviations from the trimmed values are appreciably large in comparison with the helicopter with see-saw rotor. The pitching (Θ) and yawing (Ψ) angles of the body have very large amplitudes (almost 10 degrees for pitching angle and $\pm$10 degrees for yawing angles). However the rolling angle (Φ) changes a little (almost 3 degrees).

In the diagonal penetration shown in Figure 5 (b), the tendnecy of the responses is similar to the case of the normal penetration. The responses is more mild than that of the normal penetrations to the vortex core. Since the elapsed time to penetrate the vortex core is longer than that of the normal penetration, the helicopter itself reacts very slowly to the gust velocity field. Therefore the body attitude, specifically in pitching and yawing angles, deviates very moderately with high amplitudes of the responses.

In the case of the parallel penetration shown in Figure 5 (c), the responses of the rotor hub are completely different from the other two cases. First of all, the thrust deviation is very little and others are similarly small. However, the yawing angle deviates very much from the trimmed values (almost 15 degrees in the yawing angle). This phenomena is almost same as that of the see-saw rotor's case [Ref.13]. Since the amplitude of the yawing angle of the body depends on the aerodynamic characteristics of the vertical wing , it must be paid attention to the aerodynamic chracteristics of the vertical wing operating in high angle of side slip in the analysis.

In all Figures, the spike of the response near the origin of time can be seen. This came from the step response of the helicopter because the gust velocities near the time origin were considered to be finite.

6-2 Response of helicopter with hingeless rotor

In the case of the helicopter with hingeless rotor, elastic flatwise, chordwise, torsional deformation must be taken into account because the blades are attached to the rotor hub without mechanical hinge. In the present calculations, the equivalent flapping hinge and lead-lag hinge areintroduced in the manner of section 4. However the torsional deflection is not considered in this study. The detailed dimensions and flight conditions of this helicopter are shown in Tables 1 and 3.

It was found from the calculation of the trimmed flight that the vibratory characteristics is same as that of the helicopter with articulated rotor.

Shown in Figures 6 (a), (b) and (c) are the dynamic responses of the helicopter with hingeless rotor in climbing flight (γ = 10°) for normal, diagonal and parallel penetrations to the vortex core respectively. The tendency of the dynamic responses is very similar to that of the helicopter with articulated rotor. In this case, the helicopter seems to hit the second vortex core generated by the left wing tip of the large airplane. This is resulted from the downward shift from the flight course. The horizontal and side forces greatly react to the gust velocity when the helicopter hit the vortex core. In the case of the helicopter with see-saw rotor, these forces showed change little.

In the normal penetration shown in Figure 6 (a), the attitude of the helicopter change a little except the yawing angle. Sicne the vortex core has very strong suction flow (q_x), the yawing moment due to the vertical wing has a great value when the helicopter penetrates the vortex core. The vertical acceleration (or the thrust) at the rotor hub fluctuates from 0.5g to 1.7g during the penetration of the vortex core. The helicopter excursions showed that the vertical deviation is much lager than others.

In the diagonal penetration shown in Figure 6 (b), the dynamic responses of the helicopter are mild in comparison with the normal penetration.

In the case of the parallel penetration shown in Figure 6 (c), the attitudes of the helicopter show the great changes in rolling and yawing angles of the body (almost 25 degrees and ±10 degrees respectively). According to the change of rolling angle, the helicopter shows a great sideward excursion. At the same time, the yawing angle of the body changes from negative to positive values.

6-3 Effect of the feedback system

Here let us consider two feedback systems, FSS and SFS, to alleviate the responses of a helicopter with see-saw rotor.

Shown in Figures 7 (a),(b) are the results for the equipped with these feedback systems. In Figure 7 (a), the feedback system is FSS and the input is added to the conventinal control input as equation (11). In this calculation, the values of k_β , $k_{\dot\beta}$ and $k_{\ddot\beta}$, were -0.5, -1.0, 0.0 respectively. It is clear from the results that the effect of this feedbak system on the dynamic response is little. The flpping deviation slightly reduced. The roll angle and the lateral velocity of the disturbed helicopter body are slightly improved.

In Figure 7 (b), the dynamic behaviors of the disturbed helicopter installed with the SFS are shown. From this figure, the effect of this control system on the responses of the helicopter are predominant. In this calculation, the following feedback gains were used,

$$(G_{\dot{\Delta h}},\ G_{\ddot{\Delta h}},\ G_\Theta,\ G_{\dot\Theta},\ G_{\Delta\overline{U}_X},\ G_{\Delta\dot{\overline{U}}_X},\ G_\Phi,\ G_{\dot\Phi},\ G_{\Delta\overline{U}_Y},\ G_{\Delta\dot{\overline{U}}_Y},$$
$$G_\Psi,\ G_{\dot\Psi}) = (-5.0, -1.5, -0.5, -0.5, -2.5, -1.2.$$
$$-0.2, -0.3, -0.6, -1.2, -0.5, -0.25).$$

Since the SFS system is composed of the attitude hold control and the velocity hold control, the reduction of the attitude and velocity deviation due to the trailing vortex is specifically predominant. Instead, the horizontal, lateral forces, C_H and C_Y and the flapping angle deviation increase appreciably. The hub moments, C_l and C_m are not effected by this control system. In the thrust response, the shape of the deviation is greatly changed in order to maintain the steady flight and its deviation is highly reduced.

7. CONCLUSIONS AND RECOMENDATION

The Local Momentum Theory has been extended to analyze the dynamic responses of the three types of helicopter which penetrate a pair of trailing vortices of a preceding airplane at the distance of 10,000m from the airplane. The wake vortices are assumed to be a frozen gust but disturbed by the blade motion and the helicopter dynamics is allowed to have six-degrees of freedom. The simplified feedback system is applied to alleviate the vibratory deviation of the helicopter from the trimmed flight.

The major results in this study are drawn as follows;

(1) The maximum mean-vertical-acceleration is less than 2g at the distance of more than 2,000 m from the airplane. It is degenerated by reducing the flight path angle (Ψ_W) from the normal penetration

(2) The vertical acceleration is severe in the normal penetration whereas the rolling and yawing excursions are predominant in the parallel penetration.

(3) In both the normal and diagonal penetrations, the attitude of the helicopter shows similar responses for two types of helicopter.

(4) In the parallel penetration, the rolling angle of the body attitude shows greatest amplitude for the helicopter with hingeless rotor.

(5) The dynamic responses of the helicopter penetrating the vortex wake of the large airplane strongly depends on the gust velocity field.

(6) For the simplified feedback system to alleviate the gust responses of the helicopter, the simplified feedback control system has great effect on the vibratory response reduction rather than the individual blade pitch control system.

In the present study, the calculations in the limited cases were performed. It is, however, necessary to calculate the responses of the various helicopters penetrating the trailing vortices in various flight conditions for much better understanding of this problem.

8. REFERENCES

1. Azuma, A. and Kawachi, K.; Local Momentum Theory and Its Application to the Rotary Wing. J. of Aircraft. (1979) 16(1) 6-14.
2. Kerr, T.H. and Dee, F.W.; A Flight Investigation into the Persistence of Trailing Vortices behind Large Aircraft. British A.R.C. C.P.489,(1959).
3. McCormick, B.W., Tangler, J.L. and Sherrieb, H.E.; Structure of Trailing Vortices. J. of Aircraft (1968) 5 (3) 260-267.
4. Sammonds, R.I., Stinnett, G.W.,Jr. and Larson, W.E.; Hazard Criteria for Wake Vortex Encounters. AIAA 3rd Atom. F.M. Conference (1976).
5. Nelson, R.C. and McCormick, B.W.; The Dynamic Behavior of an Aircraft Encounting Aircraft Wake Turbulence.
6. Allison, D.O. and Bobbitt, P.J.; Semiempirical Method for Predicting Vortex-Induced Rolling Moments. NASA TM 87579 (1985).
7. Dunham, R.E.,Jr., Holbrook, G.T., Mantay, W.R., Campbell, R.L. and Van Gunst, R.W.; Flight-Test Experience of a Helicopter Encountering an Airplane Trailing Vortex. 32nd Annual National V/STOL Forum of the AHS. (1976) No. 1063.
8. Mantay, W.R., Holbrook, G.T., Campbell, R.L. and Tomaine, R.L.; Flight Investigation of the Response of a Helicopter to the Trailing Vortex of a Fixed- Wing Aircraft. AIAA 3rd Atom. F.M. Conference (1976).
9. Dreier, M.E.; The Influence of a Trailing Tip Vortex on a Thrusting Rotor. A Thesis in Aerospace Engineering. The Pen. State Univ. (1977).

10. Curtiss, H.C.,Jr. and Zhou, Zheng-gen; The Dynamic Response of Helicopters to Fixed Wing Aircraft, Seminar at Nanjing Aeronautical Univ. (1985).
11. Verstynen, H.A. and Dunham, R.E.; A Flight Investigation of the Trailing Vortices Generated by a Jambo Jet Transport. NASA TN D-7172 (1973).
12. Azuma, A., Kawachi, K. and Saito, S.; The Local Momentum Method and Its application to Helicopter Aero- and Flight-Dynamics. Seminar at Nanjing Aeronautical Univ. (1985).
13. Azuma, A., Saito, S. and Kawachi, K.; Response of Helicopter Penetrating the Tip Vortices of Large Airplane. Vertica, will be published.
14. Lamb, H.; Hydrodynamics. Fifth Edition (1930).
15. Azuma, A. and Saito S.; Study of Rotor Gust Response by Means of the Local Momentum Theory. J. of A.H.S. (1982) 58-72.
16. Saito, S, Azuma, A. and Nagao, M.; Gust Response of Rotoary Wing Aircraft and Its Alleviation. Vertica (1981) 5 173-184.
17. Saito, S.; A Study of Helicopter Gust Response Alleviation by Automatic Control. NASA TM 85870 (1983).
18. Yasuda, Y.; On the Automatic Flight Control System at the Take-off and Landing Regimes of a Helicopter, Master Thesis of the Univ. of Tokyo (1973).
19. Tanabe, K.; Study of the Lateral Flight Characteristics at the Take-off and Landing Regimes of a Helicopter, Master Thesis of the Univ. of Tokyo (1974).

NOMENCLATURES

a	empirical constant of effective eddy viscosity
b	number of blades
b_A	wing span of aircraft
C_D	drag coefficient of wing
C_H	H-force coefficient
C_L	lift coefficient
C_l	rolling moment coefficient at rotor hub
$C_{MF,XB}$	coefficient of fuselage moment
$C_{MF,YB}$	coefficinet of fuselage moment
$C_{MF,ZB}$	coefficient of fuselage moment
C_m	pitching moment coefficient at rotor hub
C_Q	torque coefficient
C_T	thrust coefficient
C_Y	Y-force coefficient
D_0	profile drag of aircraft
(F_{XB},F_{YB},F_{ZB})	external forces given by eq.(7)
g	acceleration of gravity

h_H	position of horizontal wing
h_R	hub height
h_T	height of tail rotor
h_V	height of vertical wing
(I_X, I_Y, I_Z)	moments of inertia of the helicopter
I_β	moment of inertia of a blade about flapping hinge
i_S	inclination of rotor shaft
J_{XZ}	product of inertia
k_β	spring stiffness at flapping hinge
L	lift
l_H	longitudinal position of horizontal wing
l_R	hub position
l_T	longitudinal position of tail rotor
l_V	longitudinal position of vertical wing
(M_{XB}, M_{YB}, M_{ZB})	external moments given by eq.(8)
M_β	mass moment of a blade about flapping hinge
m_A	mass of aircraft
m_H	mass of helicopter
m_β	mass of blade
n	load factor
p	rolling angular velocity
q	pitching angular velocity
(q_x, q_y, q_z)	longitudinal, radial and circumferential gust components shown in Fig.1
(q_x^*, q_y^*, q_z^*)	longitudinal, radial and circumferential gust components at core center
R	rotor radius
r	radial position or yawing angular velocity
r^*	core radius of tip vortex
S	rotor disc area
S_A	wing area
T_1	transformation matrix given by Appendix A
T_2	transformation matrix given by Appendix A
t	time
U_A	flight speed of airplane
U_H	flight speed of helicopter
u	longitudinal flow speed shown in Fig.1
u_H	longitudinal flight speed of helicopter
v	lateral flow speed in Fig.1
v_H	lateral flight speed of helicopter
W	non-dimensinal weight $= m_H g/\rho S(R\Omega)^2$
w	vertical flow speed shown in Fig.1
w_H	vertical flight speed of helicopter
X_{CG}	longitudinal position of the center of gravity of helicopter
(X, Y, Z)	coordinate system fixed to airplane shown in Fig.1
(X_B, Y_B, Z_B)	coordinate system fixed to helicopter shown in Fig.1

(X_{CG}, Y_{CG}, Z_{CG})	longitudinal,lateral and vertical position of helicopter center of gravity in (X,Y,Z) coordinate system
(X_R, Y_R, Z_R)	coordinate system fixed to rotor shaft shown in Fig.1
(x, y, z)	coordinate system fixed to wing tip shown in Fig.1
x	nondimensional radial position =r/R, or horizontal distance
(X_{CG}, Y_{CG}, Z_{CG})	longitudinal,lateral and vertical position of the center of gravity of helicopter in (x,y,z) coordinate system
x_β	flapping hinge offset
$\bar{x}$	spanwise position of blade center of gravity
y	spanwise position
α	angle of attack
β	flapping angle
β_{1c}	longitudinal flapping angle
β_{1S}	lateral flapping angle
β_1	flapping angle of No.1 blade
β_0	coning angle
$\bar{\beta}0$	preconing angle
Γ	circulation
Γ_0	circulation of aircraft at midspan
γ	flight path angle of helicopter
Δ	small increment
δ_H	setting angle of horizontal wing
η	efficiency
Θ	pitching angle of helicopter body
Θ_o	initial setting angle of body frame
θ_T	blade twist angle
μ	advance ratio
ν	kinematic viscosity
ν_e	effective eddy viscosity
ρ	air density
Φ	rolling angle of helicopter body
Φ_o	initial setting angle of body frame
Ψ	yawing angle of helicopter body
Ψ_W	flight path angle of helicopter with respect to wake
Ψ_o	initial setting angle of body frame
ψ	azimuth angle
Ω	rotor rotational speed
ω	natural flapping-frequency
$(\ )_F$	quantity concerning fuselage
$(\ )_H$	quantity concerning horizontal wing or concerning helicopter
$(\ )_T$	quantity concerning tail rotor
$(\ )_V$	quantity concerning vertical wing
$(\dot{\ })$	time derivation

Appendix A. The transformation matrices, T_1 and T_2

The transformation matrices T_1 and T_2 in section 2 are given by [13]

$$T_1 = \begin{vmatrix} \cos\Theta\cos\Psi & \sin\Phi\sin\Theta\cos\Psi - \cos\Phi\sin\Psi & \cos\Phi\sin\Theta\cos\Psi + \sin\Phi\sin\Psi \\ \cos\Theta\sin\Psi & \sin\Phi\sin\Theta\sin\Psi + \cos\Phi\cos\Psi & \cos\Phi\sin\Theta\sin\Psi - \sin\Phi\cos\Psi \\ -\sin\Theta & \sin\Phi\cos\Theta & \cos\Phi\cos\Theta \end{vmatrix}$$

$$T_2 = \begin{vmatrix} \cos\Theta_o\cos\Psi_o & \cos\Theta_o\sin\Psi_o & -\sin\Theta_o \\ -\cos\Phi_o\sin\Psi_o + \sin\Phi_o\sin\Theta_o\cos\Psi_o & \cos\Phi_o\cos\Psi_o + \sin\Phi_o\sin\Theta_o\sin\Psi_o & \sin\Phi_o\cos\Theta_o \\ \sin\Phi_o\sin\Psi_o + \cos\Phi_o\sin\Theta_o\cos\Psi_o & -\sin\Phi_o\cos\Psi_o + \cos\Phi_o\sin\Theta_o\sin\Psi_o & \cos\Phi_o\cos\Theta_o \end{vmatrix}$$

and where (Ψ_o , Θ_o , Φ_o) are the inertial setting angles of the body coordinate with respect to the (X, Y, Z) coordinate.

Appendix B. External forces and moments

External forces (F_{XB}, F_{YB}, F_{ZB}) and moments (M_{XB}, M_{YB}, M_{ZB}) acting on the helicopter body are expressed as follows [13]:

$$F_{XB} = \rho S(R\Omega)^2 [C_T \sin i_S - C_H \cos i_S - \eta_T C_{HT} + C_{LF}\sin\alpha_F + C_{LH}\sin\alpha_H + C_{LV}\sin\alpha_V - C_{DF}\cos\alpha_F - C_{DH}\cos\alpha_H - C_{DV}\cos\alpha_V - \overline{W}s\sin\Theta]$$

$$-bm_\beta[u+qw-rv-R\Omega^2\{\overline{x}\beta_0+(h_R/R)\}(q/\Omega^2)] \qquad \text{(B-1)}$$

$$F_{YB} = \rho S(R\Omega)^2 \,[C_Y + \eta_T C_{TT} - C_{YF} - C_{LV}\cos\alpha_V - C_{DV}\sin\alpha_V + \overline{W}s\sin\Phi\cos\Theta]$$

$$-bm_\beta\,[v+ru-pw+R\Omega^2\{\overline{x}\beta_0+(h_R/R)\}(p/\Omega^2)] \qquad \text{(B-2)}$$

$$F_{ZB} = \rho S(R\Omega)^2 \,[-C_T\cos i_S - C_{LF}\cos\alpha_F - C_{LH}\cos\alpha_H + C_{DF}\sin\alpha_F + C_{DH}\sin\alpha_H$$

$$+C_{DV}\cos\alpha_V + \overline{W}c\cos\Phi\cos\Theta]$$

$$-bm_\beta\,[w+pv-qu+R\Omega^2(l_R/R)(q/\Omega^2)] \qquad \text{(B-3)}$$

$$M_{XB} = \rho S(R\Omega)^2 R\,[-C_l\cos i_S - C_Q\sin i_S + C_Y(h_R/R) + \eta_T C_{TT}(h_T/R) + C_{MF,XB}$$

$$-(C_{LV}\cos\alpha_V + C_{DV}\sin\alpha_V)(l_V/R)]$$

$$+bm_\beta h_R\,[-(v+ru-pw)-R\Omega^2\{\overline{x}\beta_0+(h_R/R)\}(p/\Omega^2)]$$

$$+bm_\beta(R\Omega)^2\{(1/2)x_\beta\overline{x}(p/\Omega^2)\} \qquad \text{(B-4)}$$

$$M_{YB} = \rho S(R\Omega)^2 R\,[C_m\cos i_S + (C_H\cos i_S - C_T\sin i_S)(h_R/R)$$

$$-(C_T\cos i_S + C_H\sin i_S)(l_R/R)$$

$$+\eta_T\{C_{QT} + C_{HT}\cos\alpha_F(h_T/R) - C_{HT}\cos\alpha_F(l_T/R)\}$$

$$+C_{MF,YB} - (C_{LH}\cos\alpha_H + C_{DH}\sin\alpha_H)(l_H/R)$$

$$+(C_{DH}\cos\alpha_H - C_{LH}\sin\alpha_H)(l_H/R)$$

$$-C_{DV}\sin\alpha_V(l_V/R) + C_{DV}\cos\alpha_V(h_V/R)]$$

$$+bm_\beta h_R\,[(u+qw-rv)-R\Omega^2\{\overline{x}\beta_0+(h_R/R)\}(q/\Omega^2)]$$

$$+bm_\beta(R\Omega)^2\{(1/2)x_\beta\overline{x}(q/\Omega^2)\}$$

$$-bm_\beta l_R\,[(w+pv-qu)+R\Omega^2(l_R/R)\}(q/\Omega^2)] \qquad \text{(B-5)}$$

$$M_{ZB} = \rho S(R\Omega)^2 R\ [C_Q \cos i_S - C_l \sin i_S - C_Y(l_R/R) - \eta_T C_{TT}(l_T/R) + C_{MF,ZB}$$

$$+(C_{LV}\cos\alpha_V + C_{DV}\sin\alpha_V)(l_V/R)]$$

$$-bm_\beta l_R\ [-(v+ru-pw) - R\Omega^2\{\bar{x}\beta_0 + (h_R/R)\}(p/\Omega^2)]$$

$$+bm_\beta(R\Omega)^2\ [\overline{x^2}\{-(r/\Omega^2) - (1/2)\beta_{1S}(q/\Omega^2) + (1/2)\beta_{1C}(q/\Omega^2)\}] \quad \text{(B-6)}$$

where nondimensional rotor forces and moments (C_T, C_H, C_Y, C_Q, Cl, Cm) are those including the inertial components (caused by the blade motion) as well as the aerodynamic components.

Table 1. Dimensions of the two types of helicopter

Items			Articulated	Hingeless
Gross mass	m_H	(kg)	1,089	2,850
Moment of inertia of body	I_X	(kgm²)	431	2,380
Moment of inertia of body	I_Y	(kgm²)	1,186	7,314
Moment of inertia of body	I_Z	(kgm²)	911	5,560
Hinge stiffness	$k\beta$	(Nm/rad)	0	149.0
	$k\zeta$	(Nm/rad)	0	816.0
For Main Rotor				
Rotor radius	R	(m)	4.0	5.5
Number of blades	b		4	4
Blade chord	c	(m)	0.178	0.32
Blade twist	θ_t	(deg)	-9.14	-8.0
Rotor rotational speed	Ω	(rad/s)	50.7	40.15
Blade mass	$m\beta$	(kg)	16.9	31.95
Moment of inertia of blade	$I\beta$	(kgm²)	70.6	212.66
Inclination of rotor shaft	i_s	(deg)	3.0	5.0
Hinge offset	$x\beta$		0.035	0.129
	$x\zeta$		0.0	0.145
Lock number	γ		4.40	9.63
Solidity	σ		0.0543	0.074
Preconing angle	β_0	(deg)	0.0	2.5
For Tail Rotor				
Rotor radius	R_T	(m)	0.65	0.95
Number of blades	b_T		2	2
Blade chord	c_T	(m)	0.122	0.18
Blade twist	θ_{tT}	(deg)	-8.0	0.0
Rotor rotational speed	Ω_T	(rad/s)	327.0	227.2
Blade mass	m_T	(kg)	1.2	0.94
Moment of inertia of blade	$I\beta_T$	(kgm²)	0.147	0.28
δ_3 angle	δ_{3T}	(deg)	30.0	45.0
Lock number	γ_T		1.03	3.63
Solidity	σ_T		0.12	0.12
For Horizontal Wing				
Wing area	S_H	(m²)	0.714	1.0
Span	b_H	(m)	1.703	2.5
Chord	c_H	(m)	0.419	0.4
Aspect ratio	AR_H		4.06	6.25
Efficiency	η_H		0.7	0.7
For Vertical Wing				
Wing area	S_V	(m²)	0.522	2.24
Span	b_V	(m)	1.965	1.28
Chord	c_V	(m)	0.268	1.75
Aspect ratio	AR_V		7.4	5.73
Efficiency	η_V		0.9	0.8

Table 2. Dimensions of a preceding airplane

Items		Dimensions
Wing span	b_A (m)	59.6
Wing area	S_A (m^2)	511.0
Flight speed	U_A (m/s)	94.4
Mass	m_A (kg)	3.51×10^5, 2.11×10^5

Table 3. Flight conditions of the vortex generating airplane and the disturbed helicopter

Dimensions / Figs.	m_H	$2R/b_A$	U_H/U_A	$(x_0/b_A,\ y_0/b_A,\ z_0/b_A)$	Ψ_W (deg)	γ (deg)	δ_H (deg)	ω/Ω	Flight
5-(a)	0.00516	0.134	0.322	(168.0, 0.758, -0.147)	90.0	10.0	2.0	1.03	Climb
(b)	0.00516	0.134	0.322	(168.0, 0.338, -0.133)	30.0	10.0	2.0	1.03	Climb
(c)	0.00516	0.134	0.322	(168.0, 0.0, -0.134)	0.0	10.0	2.0	1.03	Climb
6-(a)	0.0135	0.184	0.435	(168.0, 0.925, -0.188)	90.0	10.0	-1.5	1.15	Climb
(b)	0.0135	0.184	0.435	(168.0, 0.422, -0.174)	30.0	10.0	-1.5	1.15	Climb
(c)	0.0135	0.184	0.435	(168.0, 0.0, -0.200)	0.0	10.0	-1.5	1.15	Climb
7-(a)	0.0142	0.225	0.482	(168.0, 0.677, -0.03)	90.0	0.0	-3.5	1.0	Level
(b)	0.0142	0.225	0.482	(168.0, 0.677, -0.03)	90.0	0.0	-3.5	1.0	Level

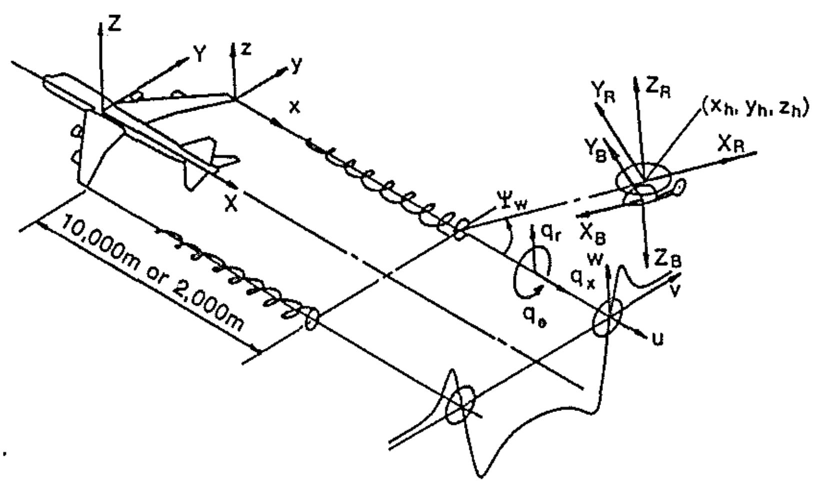

Figure 1 Geometrical relation among a vortex generating airplane, its trailing vortices and a disturbed helicopter.

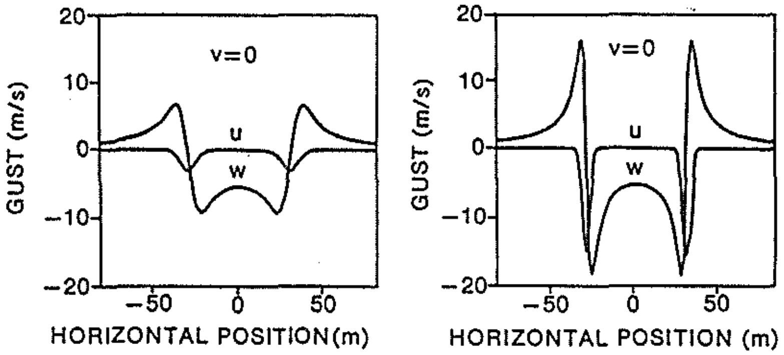

(a) At Range of 10,000m

(b) At Range of 2,000m

Figure 2 Gust profile in the airplane wake (Along a horizontal line passing through the core centers).

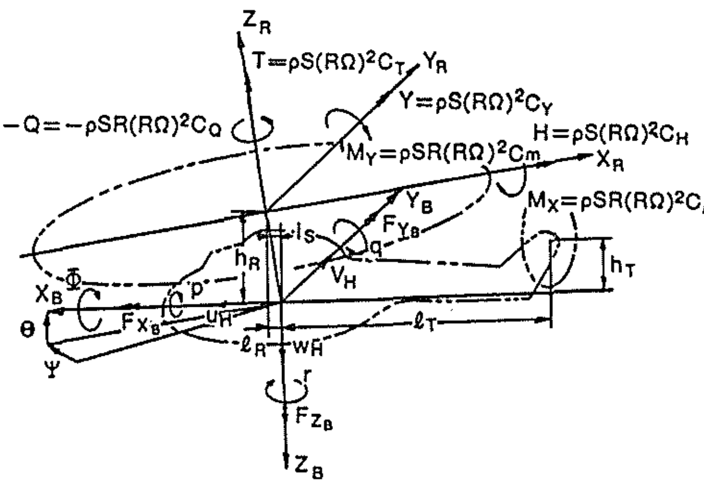

Figure 3 Forces and moments acting on the helicopter.

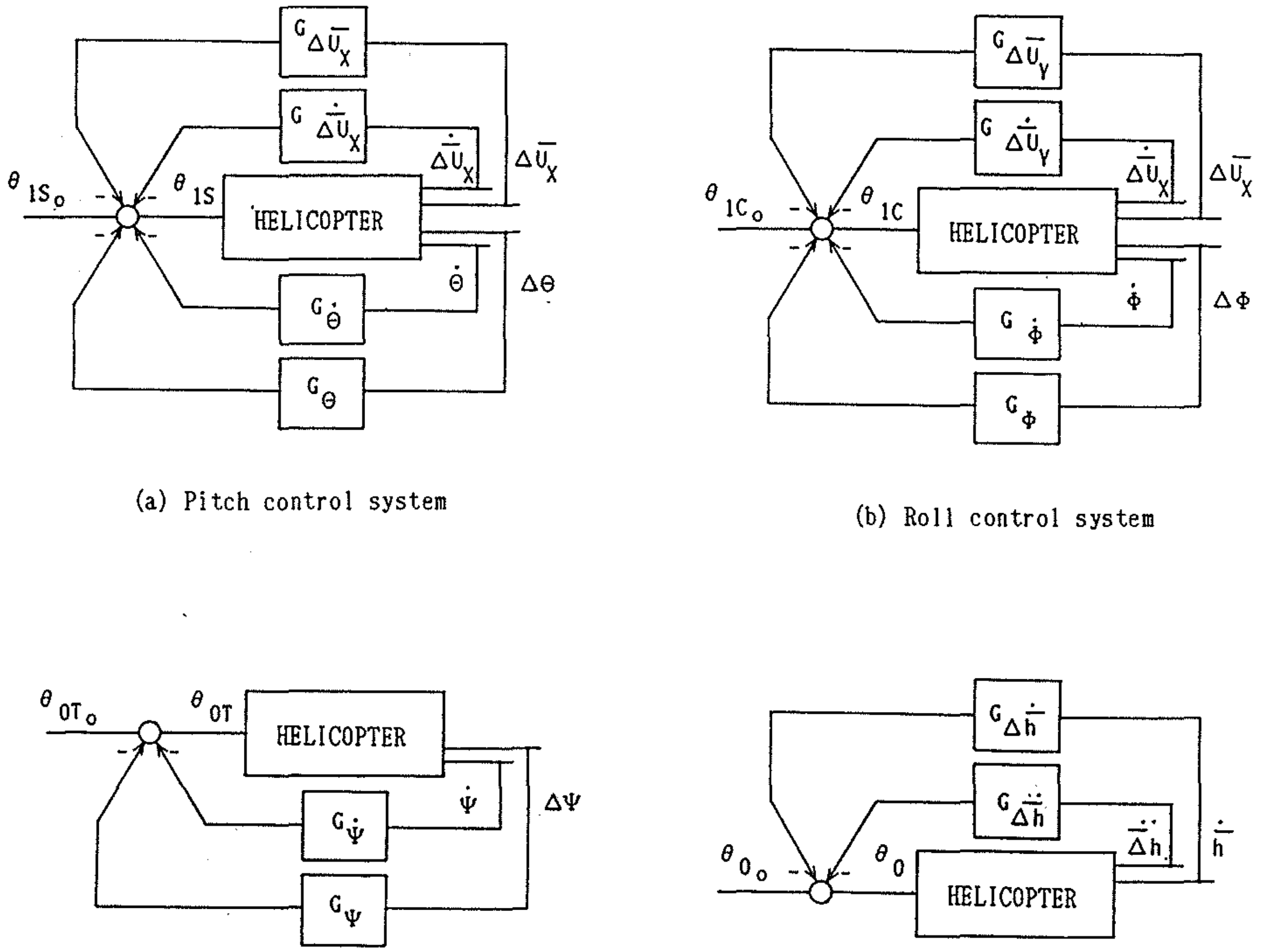

(a) Pitch control system

(b) Roll control system

(c) Yaw control system

(d) Height control system

Figure 4. Block diagrams for the control system

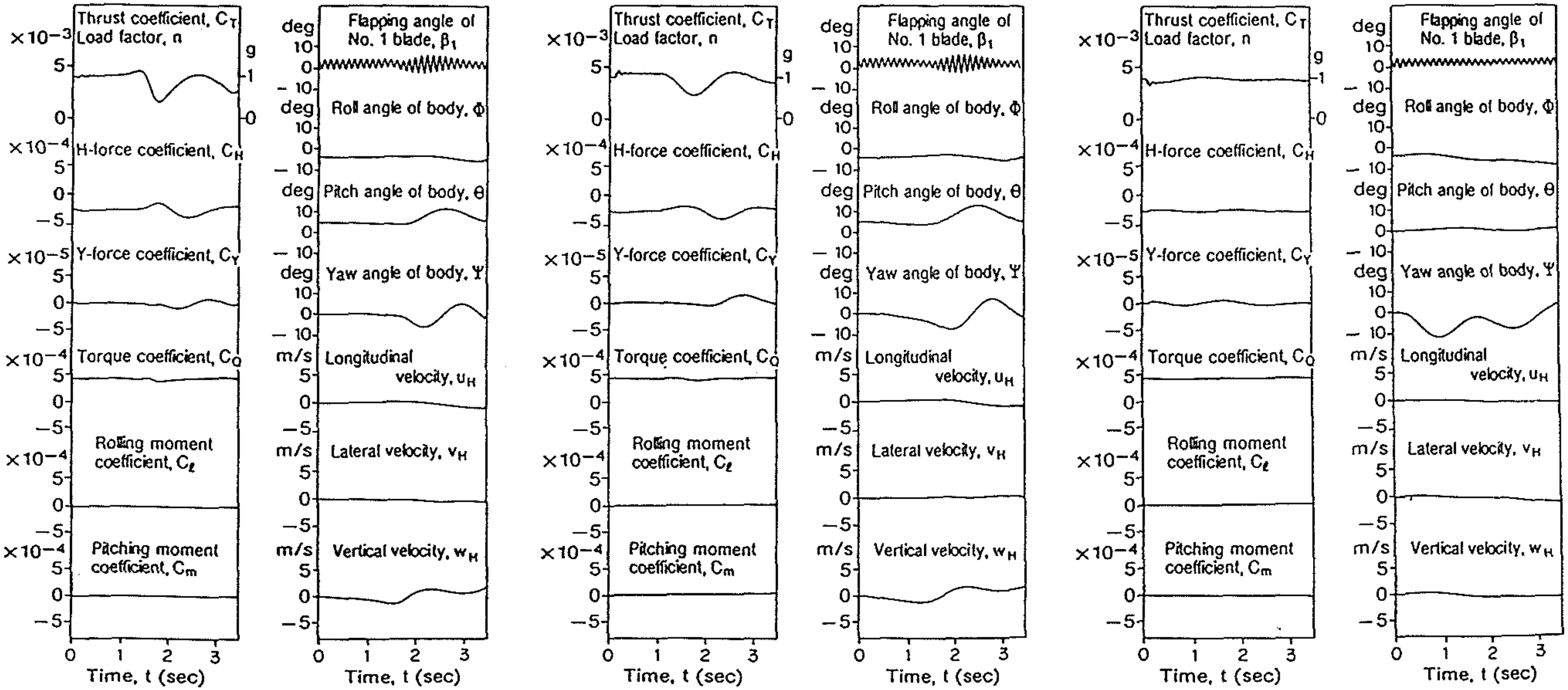

(a) Normal penetration

(b) Diagonal penetration

(c) Parallel penetration

Figure 5. Time variations of forces, moments and excursions of helicopter with articulated rotor in normal, diagonal and parallel penetrations in steady climbing flights.

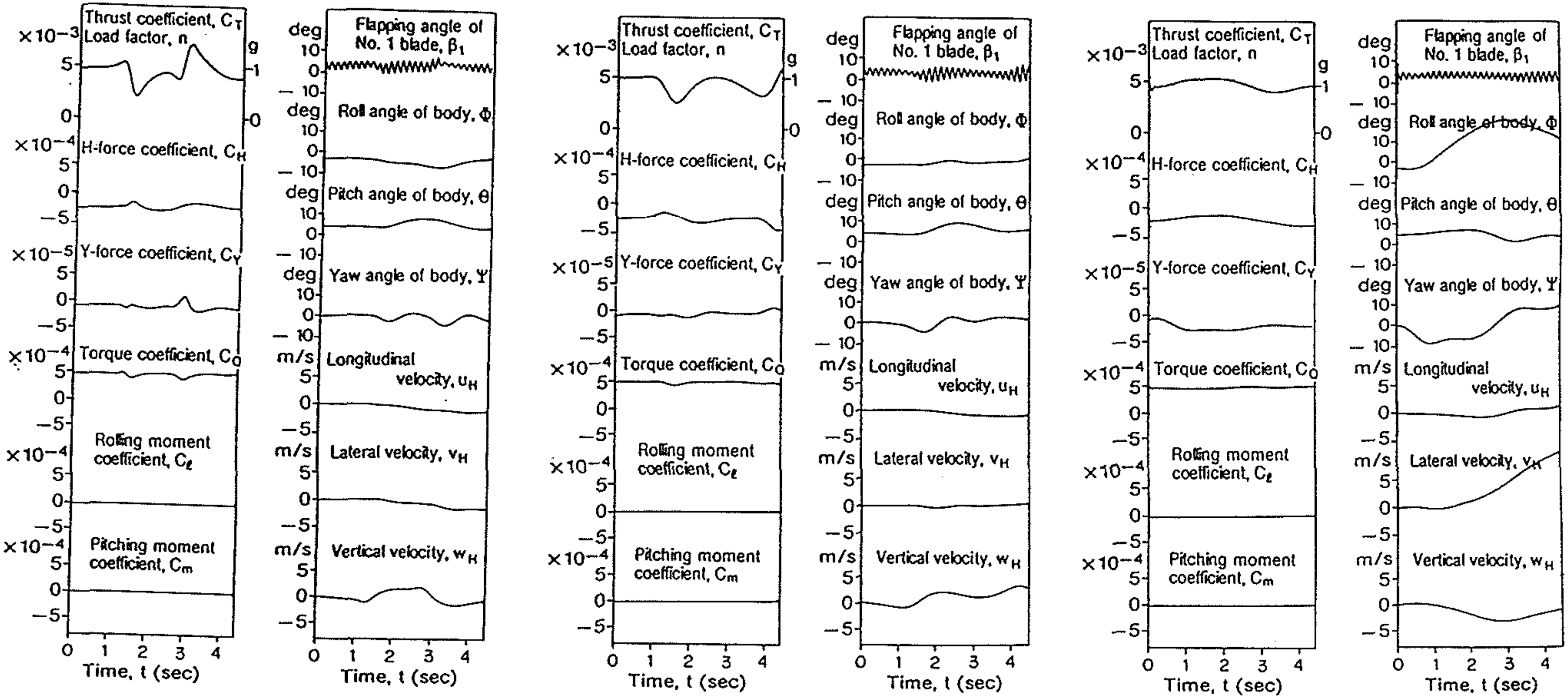

(a) Normal penetration

(b) Diagonal penetration

(c) Parallel penetration

Figure 6. Time variations of forces, moments and excursions of helicopter with hingeless rotor in normal, diagonal and parallel penetrations in steady climbing flights.

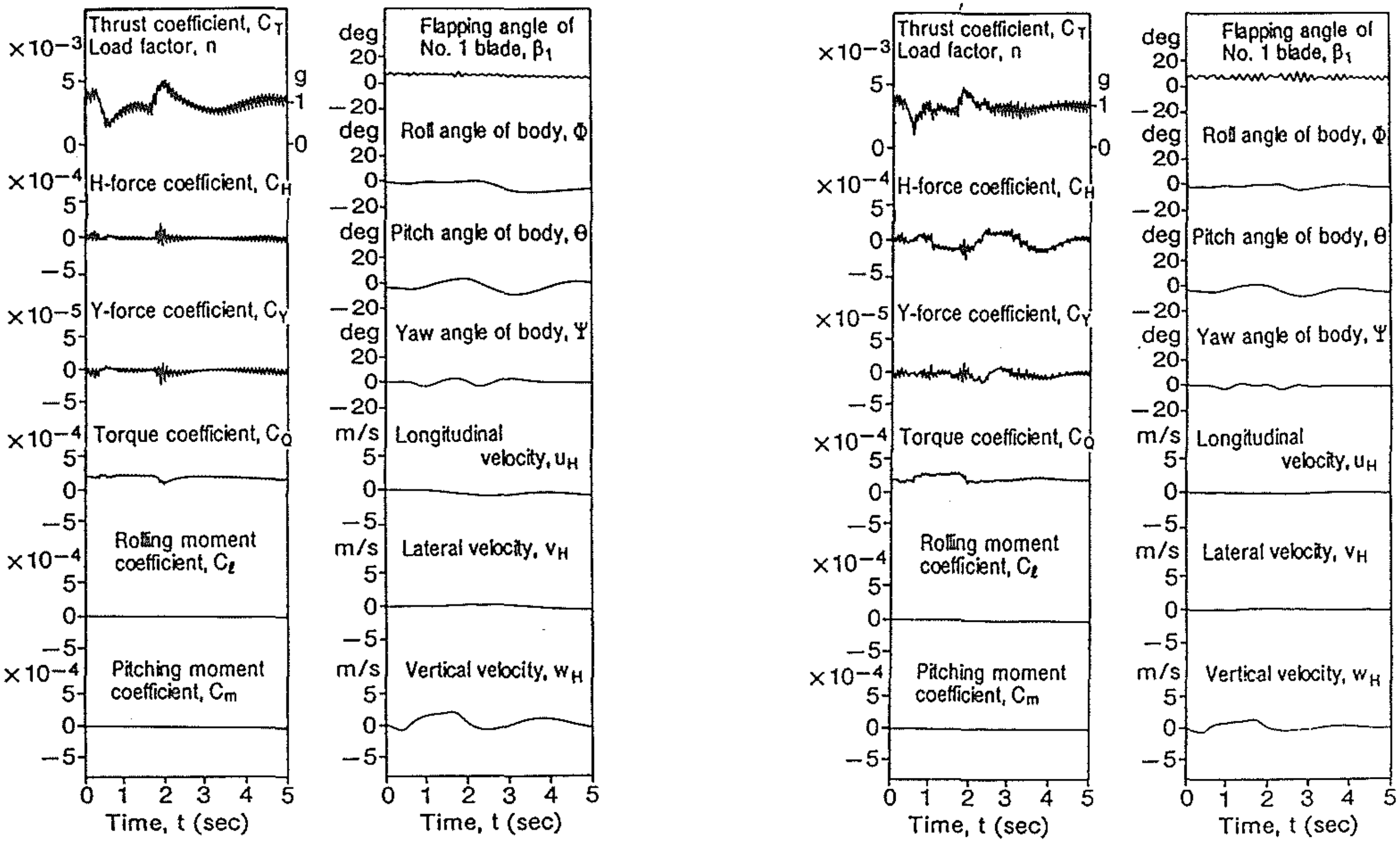

(a) Individual blade pitch control

(b) Simplified feedback control

Figure 7. Time variation of forces, moments and excursions of helicopter with see-saw rotor in level flight with simplified feedback system.